

Simulation and evaluation of perovskite solar cells utilizing various electron transport layers

R.K. Shukla, Anchal Srivastava, Shikha Rani, Nidhi Singh, Vishnu Kumar Dwivedi, Sharda Pandey, Navina Wadhvani

Physics Department, Lucknow University, Lucknow-226007, India

Corresponding author: Navina Wadhvani, navinawadhvani@gmail.com

ABSTRACT Solar cells that contain perovskite have been a significant object for consideration within the field of solar energy, consistently enhancing their efficiency year by year. In our study, we devised a novel architectural configuration for a tin-based perovskite solar cell, incorporating FTO/ZnO/CH₃NH₃SnI₃/Spiro-OMeTAD/Au. Our investigation into the working of this solar cell involved the utilization of the SCAPS-1D, a versatile tool tailored for the analysis of solar cell behavior. Through this simulation software, we explored different electron-transporting layer (ETL) materials and made adjustments to multiple parameters, including ETL and absorber layer thickness. The outcomes of our research produced promising results, showcasing significant enhancements in different solar cell parameters. These favorable findings underscore the growing allure and potential of perovskite solar cells within the realm of renewable energy. The reported CH₃NH₃SnI₃-based PSCs provide a viable path to the implementation of environmentally benign, low-cost, and high-efficiency PSCs.

KEYWORDS solar cells, perovskite, electron transporting material, SCAPS, ZnO

ACKNOWLEDGEMENTS The authors extend their sincere appreciation to Professor Marc Burgelman of Gent University for graciously supplying the software in this research work.

FOR CITATION Shukla R.K., Srivastava A., Rani S., Singh N., Dwivedi V.K., Pandey S., Wadhvani N. Simulation and evaluation of perovskite solar cells utilizing various electron transport layers. *Nanosystems: Phys. Chem. Math.*, 2024, **15** (1), 135–146.

1. Introduction

The evolution of solar cell technology has passed through distinct phases. The first generation was characterized by the utilization of crystalline and amorphous inorganic materials, exemplified by silicon (Si) and gallium arsenide (GaAs) solar cells. In the second generation, thin-film nanocrystalline solar cells like copper indium gallium selenide and cadmium telluride were introduced. The transition to the third generation marked the emergence of diverse solar cell technologies, encompassing organic, hybrid, nanostructures/quantum dots, and electrochemical (semiconductor/liquid junction) solar cells, including perovskite, plastic, and dye-sensitized solar cells [1–7].

Solar Cells based on perovskite represent a promising alternative to conventional solar cell technologies. Their appeal lies in the cost-effectiveness of their materials and their ability to produce a high number of solar cells using minimal resources, owing to the thin profile of the absorber layer. Significantly, these solar cells are eco-friendly and devoid of lead, positioning them as potential successors to silicon solar cells in the future. This research is dedicated to the investigation of lead-free and environmentally conscious solar cell technologies, employing the SCAPS-1D software for simulations.

Over the years, perovskite solar cells (PSC) have made substantial advancements, with their photoelectric power conversion efficiency (PCE) experiencing significant growth, progressing from 3.80 % in 2003 [8] to an impressive 25.70 % in 2022 [9]. This remarkable progress positions them as frontrunners for the 4th generation of solar cell technologies.

PSCs offer a multitude of advantages when compared with conventional silicon-based solar cells:

- i) PSCs demonstrated remarkable PCEs that exceed 25.00 %, bringing them near the power conversion efficiency levels of commercial Si-solar cells [10].
- ii) The production of PSCs can be achieved using cost-effective solution-based methods such as spin-coating or printing techniques. This potential reduction in manufacturing costs stands in contrast to the complex and expensive processes required for silicon solar cells [11].
- iii) Perovskite materials provide the unique ability to tune their bandgap by adjusting their composition, enabling the absorption of a wider spectrum of solar radiation. This tunability makes PSCs suitable for both single-junction and tandem solar cell configurations [12].
- iv) PSCs manufactured on different types of substrates, like flexible and lightweight materials, simplifying their integration into diverse applications such as building-integrated photovoltaics, wearable electronics, and portable devices [13].

PSCs hold significant potential for achieving efficient and profitable solar energy conversion. With ongoing research and development efforts, these cells have the potential to revolutionize the field of photovoltaics and contribute to the widespread adoption of renewable energy sources [14–21].

Several simulation models, including SCAPS, AMPS, GPVDM, and others, are available for simulating solar cells. These models analyze the properties of different layers within solar cells and their respective roles in optimizing overall solar cell performance. SCAPS, is a numerical simulation program operating in one dimension, incorporating seven layers. It was established by a team of researchers specializing in solar cells at the University of Gent. Comprehensive information about the program employed can be found in the literature [22–25].

Choosing to simulate and evaluate perovskite solar cells utilizing various electron transport layers is a strategic decision with several merits. Firstly, perovskite solar cells have emerged as promising candidates for efficient and cost-effective solar energy conversion. By simulating their performance, we gain valuable insights into optimizing their efficiency and stability. The focus on different electron transport layers is particularly relevant because the choice of this layer significantly influences the overall performance of the solar cell. Through simulation, we can systematically assess the impact of various electron transport materials on key parameters like charge transport, recombination rates, and overall device efficiency. Simulating these scenarios provides a cost-effective and time-efficient way to explore a wide range of possibilities, aiding in the identification of optimal electron transport layers for enhanced device performance. This research is crucial for advancing the understanding of perovskite solar cells and contributes to the ongoing efforts to make solar energy more accessible and sustainable. Ultimately, the chosen simulation approach allows for a comprehensive evaluation that can guide experimental efforts toward more efficient and stable perovskite solar cell designs.

2. The elaborate structure of perovskite solar cells

Perovskite is a mineral comprising Calcium, Titanium, and Oxygen with the chemical formula CaTiO_3 . In a more comprehensive context, the term 'perovskite structure' refers to any compound that possesses the ABX_3 composition and shares crystallographic characteristics resembling those of the Perovskite mineral. In this context, 'A' signifies an organic cation, 'B' denotes a larger inorganic cation, and 'X₃' indicates a somewhat smaller halogen anion.

The conventional perovskite solar cell adopts an n-i-p type configuration, where 'n' represents the electron-conductive layer, 'i' signifies the absorber layer, and 'p' serves as the hole-conductive layer. For our study, we opted for $\text{CH}_3\text{NH}_3\text{SnI}_3$ as the absorber layer, and we conducted a systematic evaluation of Electron Transport Layer (ETL) by choosing materials from a range of options, including zinc oxide (ZnO), La-doped BaSnO₃ (LBSO), Tin(IV) oxide (SnO_2), Ceric oxide (CeO_2), Phenyl-C61-butiric acid methyl ester (PCBM), Tungsten trioxide (WO_3), Indium Gallium Zinc Oxide (IGZO), Cadmium sulfide (CdS), Copper monoxide (CuO), and Buckminsterfullerene (C60). The hole-conductive layer (HTL) utilized in our design is 2,2',7,7'-Tetrakis(N,N-di-p-methoxyphenylamine)9,9'-spirobifluorene (Spiro-OMeTAD). Fig. 1 provides an illustration of the perovskite solar cell architecture under investigation, and Table 1 offers essential material parameters necessary for conducting the simulation.

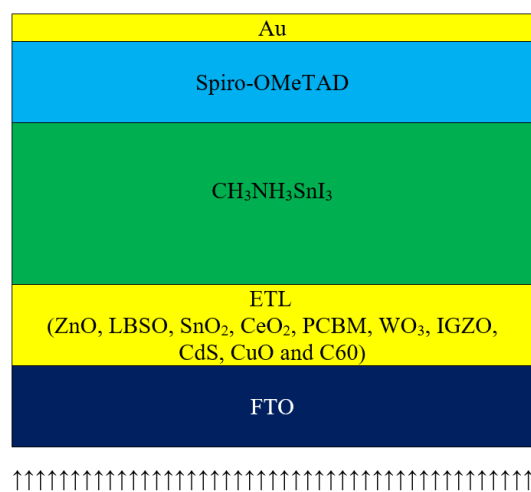


FIG. 1. The architecture of the studied PSC

TABLE 1. Parameters of the materials used in simulation

Parameters	FTO	ZnO	CH ₃ NH ₃ SnI ₃	Spiro-OMeTAD
t (nm)	250	50	500	50
E_g (eV)	3.2	3.3	1.30	3.2
η (eV)	4.4	3.9	4.2	2.10
ϵ_r (relative)	9.0	9.0	10	3.0
N_c (cm ⁻³)	2.2·10 ¹⁸	1·10 ¹⁹	1·10 ¹⁸	2.5·10 ¹⁸
N_v (cm ⁻³)	1.8·10 ¹⁹	10 ¹⁹	1·10 ¹⁸	1.85·10 ¹⁹
V_{nt} (cm/s)	1·10 ⁷	1·10 ⁷	1·10 ⁷	1·10 ⁷
V_{pt} (cm/s)	1·10 ⁷	1·10 ⁷	1·10 ⁷	1·10 ⁷
μ_n (cm ² /Vs)	20	50	1.6	2·10 ⁴
μ_p (cm ² /Vs)	10	0.5	1.6	2·10 ⁴
N_D (cm ⁻³)	1·10 ²¹	5·10 ¹⁷	—	0
N_A (cm ⁻³)	0	0	3.21·10 ¹⁵	1·10 ²⁰
N_t (cm ⁻³)	1·10 ¹⁵	1·10 ¹⁵	4.5·10 ¹⁶	1·10 ¹⁴
Reference	[26]	[27]	[28]	[29]

3. Results and discussion

SCAPS-1D is specifically designed for the analysis of solar cells, developed by the University of Gent, Belgium. When configuring the input data for the Electron Transport Material (ETM), Table 2 provides a comprehensive listing of all the requisite ETM parameters essential for executing the simulation.

3.1. Effect of the electron transporting layer

In this section, we carried out an evaluation of various ETMs for solar cells, including ZnO, LBSO, SnO₂, CeO₂, PCBM, WO₃, IGZO, CdS, CuO, and C60. Fig. 2 presents a performance comparison, clearly indicating that ZnO outperforms the other materials, exhibiting the highest power conversion efficiency. As a result, ZnO was identified as the optimal electron-transport material. The photovoltaic (PV) parameters for the ZnO layer are as follows: $V_{OC} = 0.81$ V, $J_{SC} = 29.80$ mA·cm⁻², Fill Factor = 67.29 %, and PCE = 16.26 % at a thickness of 50 nm for the electron transport layer. This choice underscores the effectiveness of ZnO in significantly enhancing the overall performance.

3.2. Impact of electron transport layer thickness on solar cell performance

The primary objective of this simulation is to determine the optimal thickness that results in the most favorable attributes for the PSC. Fig. 3 depicts the simulated parameters of the PSC as the thickness of the perovskite material varies. Specifically, we varied the thickness of the electron transporting layer (ETL) within a range of 10 to 300 nm. The results indicate that the open-circuit voltage (V_{OC}) remains relatively consistent, regardless of the ETL thickness. The value of J_{SC} initially increases up to 30 nm, followed by a subsequent decrease. The FF initially rises as the ETL thickness increases up to 40 nm, after which the value of FF stabilizes. Additionally, the PCE improves as the ETL thickness increases up to 40 nm but starts to decline beyond this point. Based on these findings, we selected an electron transporting layer thickness of 40 nm for further simulations, as it represents a favorable balance of performance characteristics. At this thickness, the solar cell exhibits the solar cell parameters: $V_{OC} = 0.81$ V, $J_{SC} = 29.81$ mA·cm⁻², FF = 67.29 %, and PCE = 16.27 %.

3.3. Influence of electron transport layer donor density (N_D) variation

In this simulation, we opted for various N_D values to investigate their influence on PSCs functioning. Fig. 4 visually represents the changes in solar cell parameters in relation to the logarithm of N_D . All parameter values exhibit fluctuations in response to defect density changes. The V_{OC} initially remains constant, then rises, and finally decreases as the electron transport layer donor density increases from 1 to 1·10²² cm⁻³. Similarly, the J_{SC} remains constant up to N_D equal to

TABLE 2. Physical parameters of different ETL materials

Material	LBSO	TiO ₂	ZnO	FTO	SnO ₂	CeO ₂	PCBM	WO ₃
t (nm)	50	50	50	50	50	50	50	50
E_g (eV)	3.12	3.2	3.3	3.2	3.5	3.5	2	2.6
η (eV)	4.4	4	4	4	4	4.6	3.9	3.8
ϵ_r	22	9	9	9	9	9	3.9	4.8
N_c (cm ⁻³)	$1.8 \cdot 10^{20}$	$1 \cdot 10^{19}$	$3.7 \cdot 10^{18}$	$2.2 \cdot 10^{18}$	$4.36 \cdot 10^{18}$	$1 \cdot 10^{20}$	$2.5 \cdot 10^{21}$	$2.2 \cdot 10^{21}$
N_v (cm ⁻³)	$1.8 \cdot 10^{20}$	$1 \cdot 10^{19}$	$1.8 \cdot 10^{19}$	$1.8 \cdot 10^{19}$	$2.52 \cdot 10^{19}$	$2 \cdot 10^{21}$	$2.6 \cdot 10^{21}$	$2.2 \cdot 10^{21}$
V_{nt} (cm·s ⁻¹)	$1 \cdot 10^7$	$1 \cdot 10^7$	$1 \cdot 10^7$	$1 \cdot 10^7$	$1 \cdot 10^7$	$1 \cdot 10^7$	$1 \cdot 10^7$	$1 \cdot 10^7$
V_{pt} (cm·s ⁻¹)	$1 \cdot 10^7$	$1 \cdot 10^7$	$1 \cdot 10^7$	$1 \cdot 10^7$	$1 \cdot 10^7$	$1 \cdot 10^7$	$1 \cdot 10^7$	$1 \cdot 10^7$
μ_n (cm ² V ⁻¹ s ⁻¹)	0.69	0.02	100	20	20	100	0.2	30
μ_p (cm ² V ⁻¹ s ⁻¹)	0.69	2	25	10	10	25	0.2	30
N_D (cm ⁻³)	$2 \cdot 10^{21}$	$1 \cdot 10^{12}$	$1 \cdot 10^{18}$	$1 \cdot 10^{19}$	$1 \cdot 10^{18}$	$1 \cdot 10^{21}$	$2.93 \cdot 10^{17}$	$6.35 \cdot 10^{17}$
N_A (cm ⁻³)	—	—	—	—	—	—	—	—
N_t (cm ⁻³)	$1 \cdot 10^{15}$	$1 \cdot 10^{15}$	$1 \cdot 10^{15}$	$1 \cdot 10^{15}$	$1 \cdot 10^{15}$	$1 \cdot 10^{15}$	$1 \cdot 10^{15}$	$1 \cdot 10^{15}$
Reference	[30]	[31]	[27]	[26]	[31]	[36]	[31]	[32]

Material	IGZO	CdS	CuO	C60
t (nm)	50	50	50	50
E_g (eV)	3.05	2.4	1.5	1.7
η (eV)	$4.16 \cdot 10^{18}$	4.18	4.07	3.9
ϵ_r	10	10	18.1	4.2
N_c (cm ⁻³)	$5 \cdot 10^{18}$	$5 \cdot 10^{18}$	$2.2 \cdot 10^{19}$	$8 \cdot 10^{19}$
N_v (cm ⁻³)	$5 \cdot 10^{18}$	$5 \cdot 10^{18}$	$5.5 \cdot 10^{20}$	$8 \cdot 10^{19}$
V_{nt} (cm·s ⁻¹)	$1 \cdot 10^7$	$1 \cdot 10^7$	$1 \cdot 10^7$	$1 \cdot 10^7$
V_{pt} (cm·s ⁻¹)	$1 \cdot 10^7$	$1 \cdot 10^7$	$1 \cdot 10^7$	$1 \cdot 10^7$
μ_n (cm ² V ⁻¹ s ⁻¹)	15	100	100	$8 \cdot 10^{-2}$
μ_p (cm ² V ⁻¹ s ⁻¹)	0.1	25	0.1	$3.5 \cdot 10^{-3}$
N_D (cm ⁻³)	$1 \cdot 10^{18}$	$1 \cdot 10^{15}$	$1 \cdot 10^{15}$	$1 \cdot 10^{17}$
N_A (cm ⁻³)	—	—	—	—
N_t (cm ⁻³)	$1 \cdot 10^{15}$	$1 \cdot 10^{15}$	$1 \cdot 10^{15}$	$1 \cdot 10^{15}$
Reference	[33]	[34]	[34]	[35]

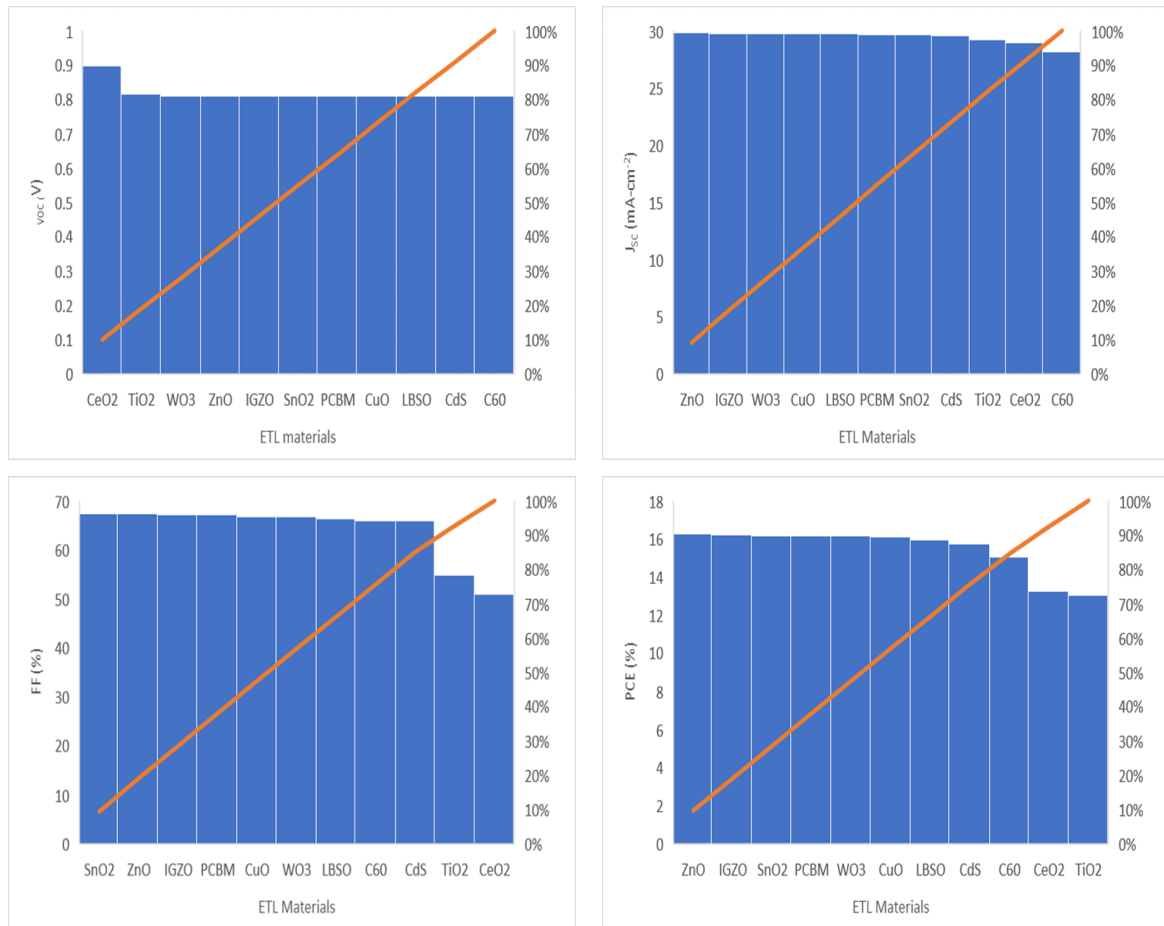


FIG. 2. Performance of PV parameters of different ETL materials

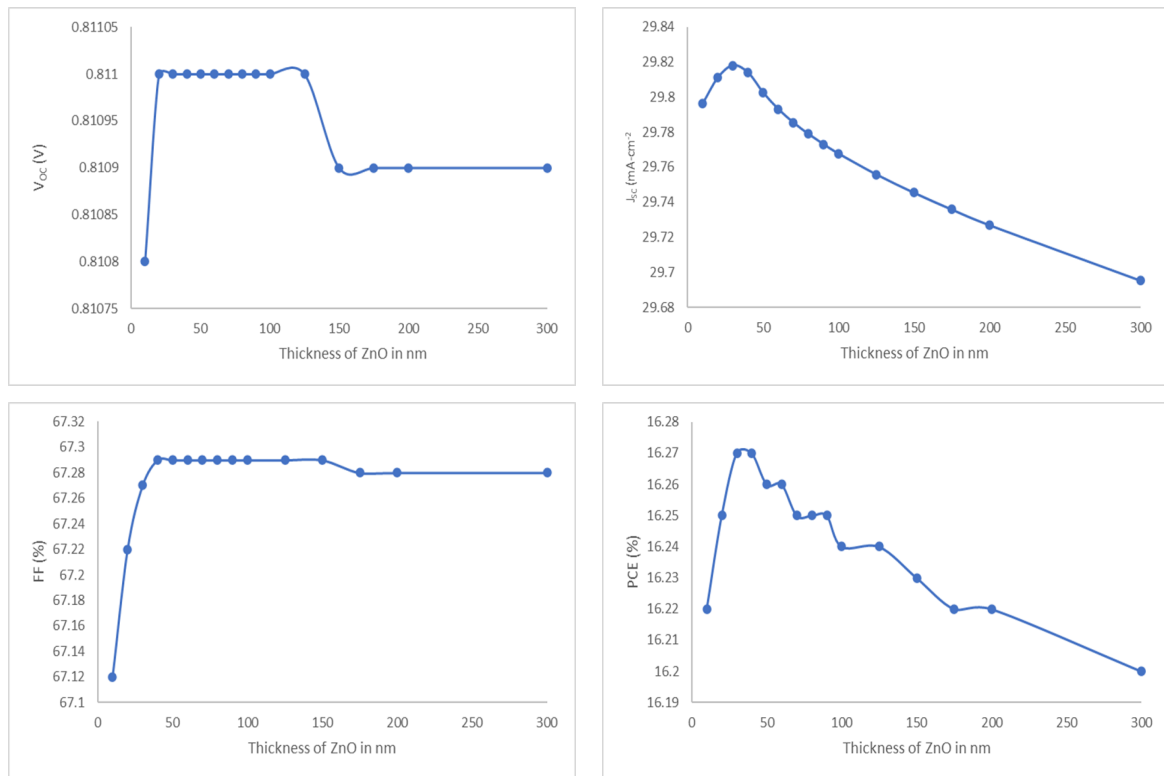


FIG. 3. Effects of ZnO thickness on PSC performance

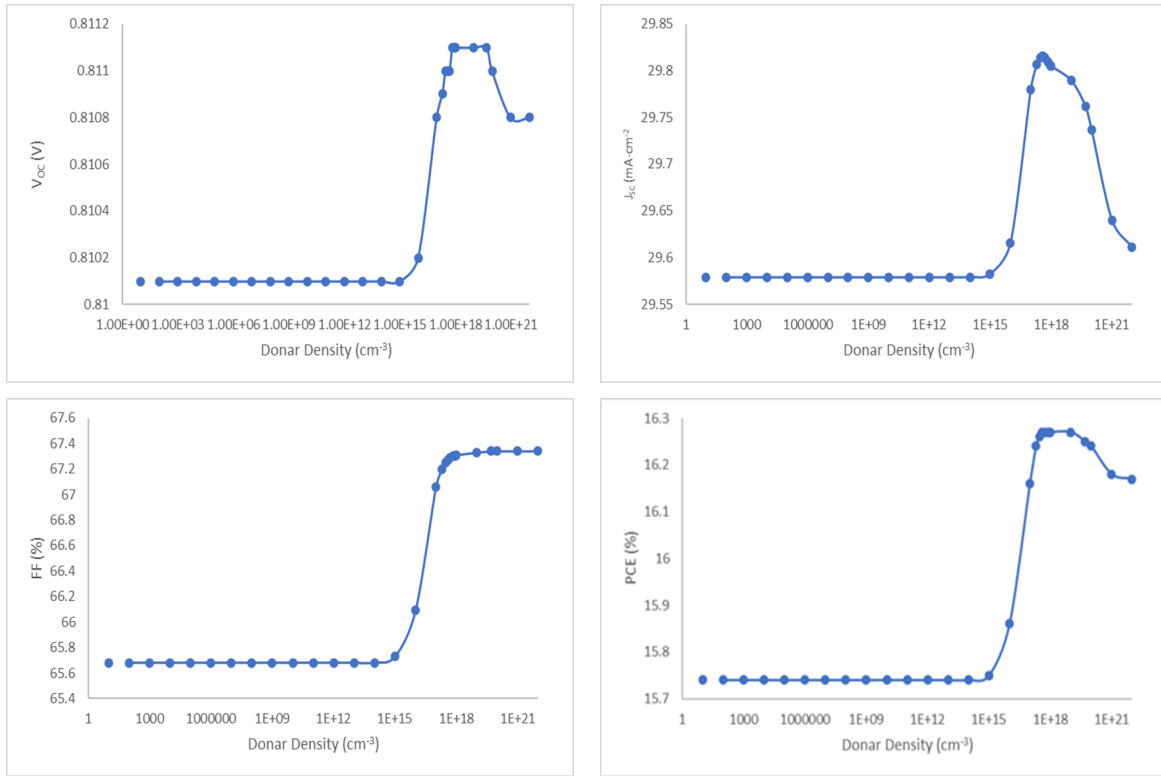


FIG. 4. Illustrates the influence of ZnO donor density (N_D) on PSC functioning

$1 \cdot 10^{13} \text{ cm}^{-3}$, then increases as N_D increases to $1 \cdot 10^{18} \text{ cm}^{-3}$, followed by a decrease. The fill factor remains constant up to N_D value of 10^{14} cm^{-3} , then increases as N_D increases to $1 \cdot 10^{19} \text{ cm}^{-3}$ and finally becomes stable. The power conversion efficiency remains constant at 15.74 % as N_D rises to $1 \cdot 10^{14} \text{ cm}^{-3}$, then power conversion efficiency rises to 16.27 % as N_D rises to $1 \cdot 10^{19} \text{ cm}^{-3}$ but decreases subsequently. Consequently, we identify the optimal value of N_D as $4 \cdot 10^{17} \text{ cm}^{-3}$ for further calculations.

3.4. Impact of absorber layer thickness on cell functioning

In this section, we explored the influence of varying the thickness of the absorber sheet $\text{CH}_3\text{NH}_3\text{SnI}_3$, ranging from 50 to 3000 nm, on the performance of the solar cell. The outcomes revealed intriguing trends in the solar cell's performance metrics. As the absorber film's thickness increased, the V_{OC} exhibited a decline until the absorber film thickness reached 500 nm, at which point V_{OC} stabilized at approximately 0.81 V. The J_{SC} initially rose from 9.86 to 30.15 $\text{mA} \cdot \text{cm}^{-2}$, reaching its peak for the absorber film thickness of 1200 nm, but as the absorber film thickness increased further the J_{SC} began to decrease. Concurrently, the FF demonstrated a continuous decrease, spanning from 79.62 to 65.87 % with increasing thickness of the absorber layer. The PCE exhibited an increase from 6.72 to 16.27 % for the 50 to 500 nm thickness of the absorber layer, followed by a slight decline to 16.11 % as the absorber layer thickness increased beyond 500 nm, as depicted in Fig. 5. At a thickness of 500 nm, the PV parameters were as follows: $V_{OC} = 0.81 \text{ V}$, $J_{SC} = 29.81 \text{ mA} \cdot \text{cm}^{-2}$, Fill Factor = 67.27 %, and PCE = 16.27 %. These findings led us to select an absorber thickness of 500 nm for further simulations, as it offered an optimal balance of performance characteristics.

3.5. Influence of varying acceptor density (N_A) in the absorber layer on cell performance

The presence of defects has a substantial impact on the optimization of device performance. Higher concentrations of defects in the absorber layer result in increased recombination due to the formation of pinholes, faster degradation of the film, and reduced stability, leading to an overall deterioration in device performance. To ascertain the ideal defect concentration in the absorber layer for optimal parameters, simulations were carried out, varying the defect density from 10 to $1 \cdot 10^{22} \text{ cm}^{-3}$.

Figure 6 illustrates that in order to achieve higher efficiency, it is essential to reduce defects in the perovskite to $8 \cdot 10^{15} \text{ cm}^{-3}$. At this optimal defect concentration, the solar cell exhibited the following parameters: $V_{OC} = 0.83 \text{ V}$, $J_{SC} = 29.63 \text{ mA} \cdot \text{cm}^{-2}$, Fill Factor = 68.48 %, and PCE = 16.91 %. These findings underscore the importance of minimizing defects in the absorber layer to enhance the total performance of the device.

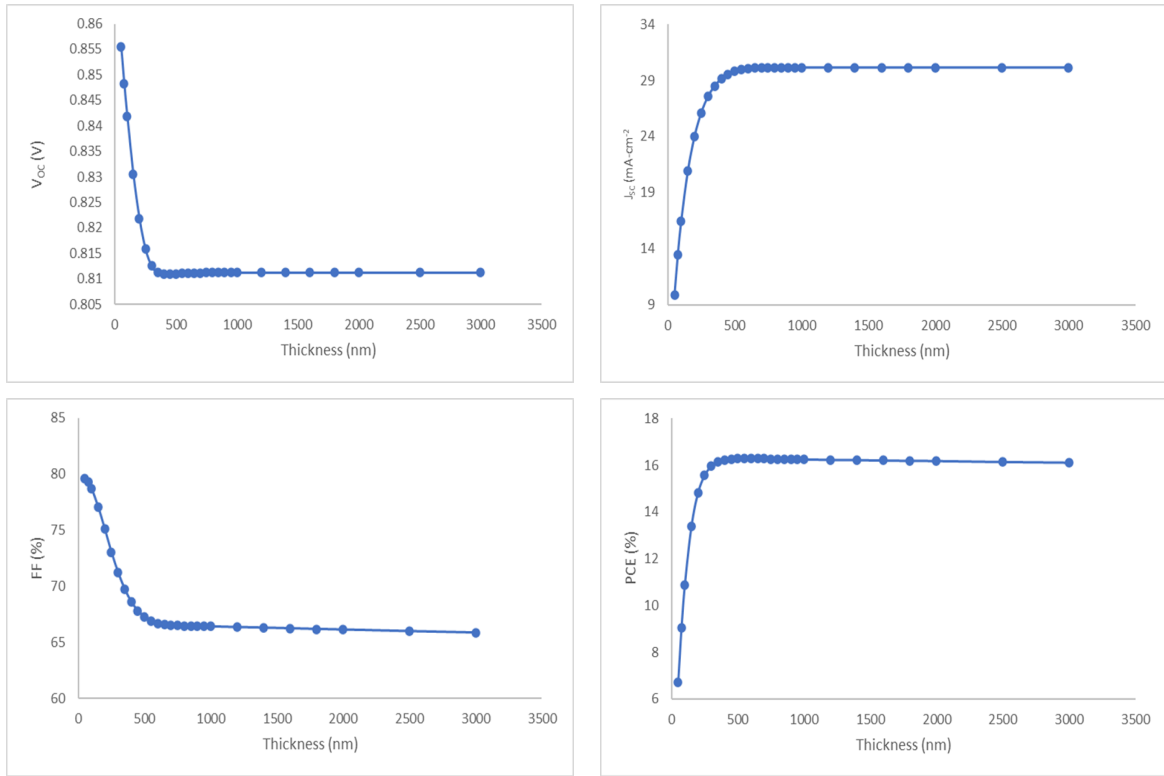


FIG. 5. Influence of $\text{CH}_3\text{NH}_3\text{SnI}_3$ thickness on PSC performance

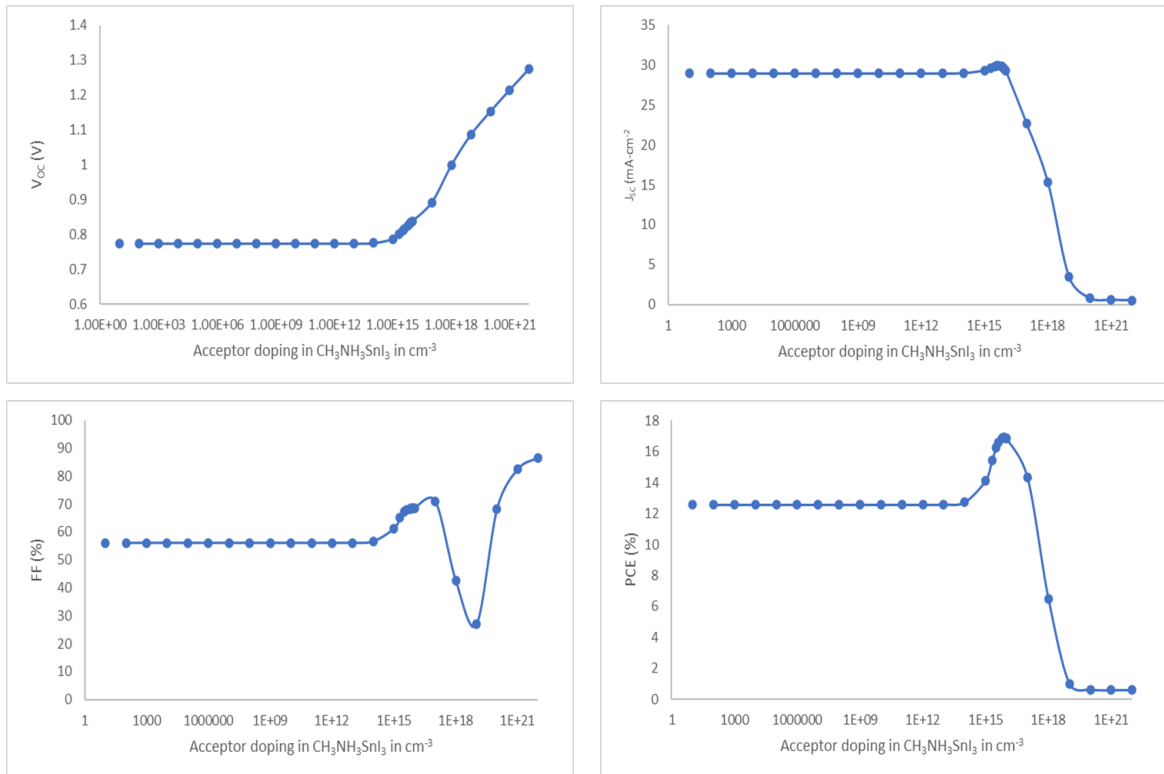


FIG. 6. Illustrates the influence of $\text{CH}_3\text{NH}_3\text{SnI}_3$ acceptor density (N_A) on PSC performance

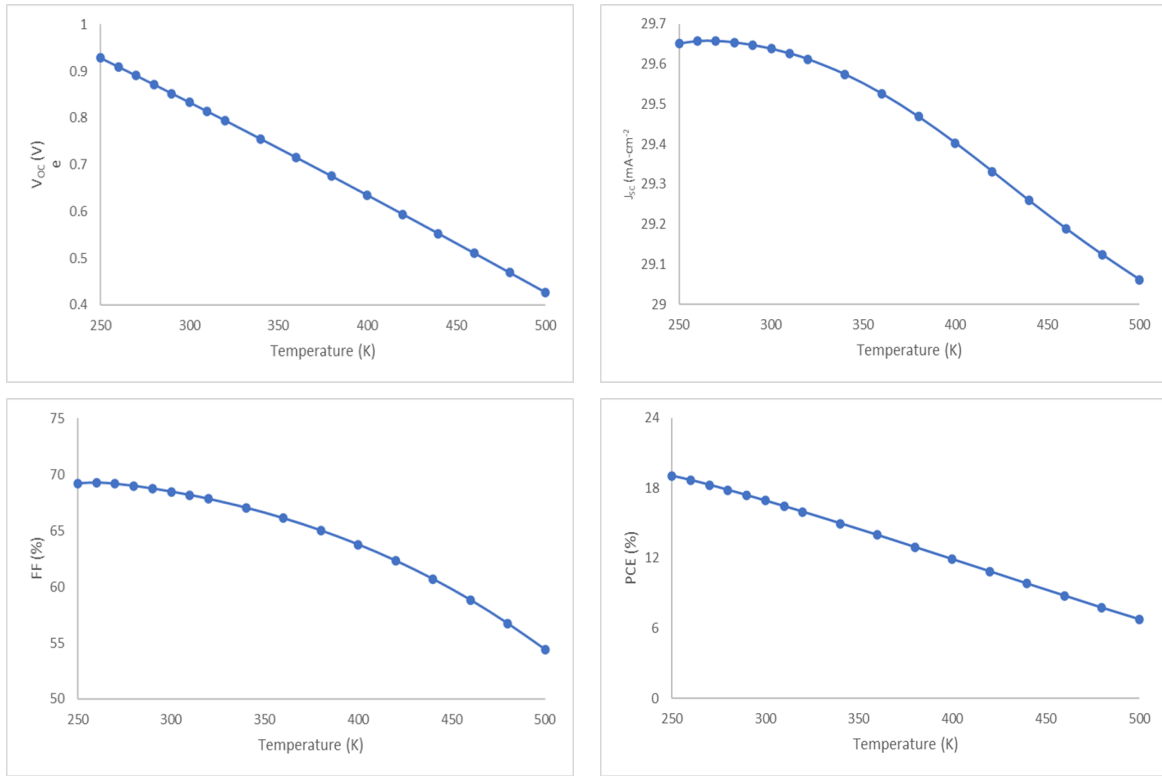


FIG. 7. Variations in solar cell characteristics with changing temperature

3.6. Influence of temperature on cell performance

Much like other semiconductor devices, solar cells are susceptible to temperature fluctuations, especially when deployed outdoors, where temperatures can surpass 300 K. It is crucial to examine how temperature affects the performance of solar cells. Fig. 7 provides insights into the variations in V_{OC} , J_{SC} , Fill Factor, and PCE at different temperatures. With an increase in temperature from 250 to 500 K, there is a notable decline in PCE, plummeting from 19.04 % to 6.76 %. At 300 K, the solar cell demonstrates the following performance parameters: $V_{OC} = 0.83$ V, $J_{SC} = 29.63$ $\text{mA}\cdot\text{cm}^{-2}$, Fill Factor = 68.48 %, and PCE = 16.91 %. These findings underscore the significance of considering and optimizing solar cell performance across varying temperature conditions.

3.7. Influence of series resistance on cell performance

The presence of series resistance plays a pivotal role in influencing the behavior of solar cells, stemming from the metal contacts on both the solar cell and layer surfaces. To evaluate the solar cell's efficiency, we systematically adjusted the series resistance within a range of 0 to 12 $\text{Ohm}\cdot\text{cm}^2$. Fig. 8 provides a visual representation of the outcomes, showing that as the series resistance increases, both J_{SC} and Fill Factor decrease, resulting in higher leakage currents and subsequently leading to reduced PCE. Interestingly, the V_{OC} exhibits relative stability across this spectrum of series resistance values.

3.8. Effect of shunt resistance on cell performance

A solar cell with a low shunt resistance experiences elevated power losses since it permits the light-generated current to deviate along an alternative route. As illustrated in Fig. 9, the fill factor (FF) is the parameter most influenced by this situation, yielding higher values for both V_{OC} and PCE, while the J_{SC} remains relatively unaffected.

3.9. Optimized short-circuit photocurrent density and open-circuit photovoltage curve

After establishing and maintaining the optimized values for both the thickness of the ETL and the absorber layer, along with the defect density, we determined the resulting photovoltaic (PV) parameters: $V_{OC} = 0.83$ V, J_{SC} of 29.63 $\text{mA}\cdot\text{cm}^{-2}$, FF = 68.48 %, and PCE = 16.91 %. Fig. 10 visually depicts the optimized current density versus voltage relationship.

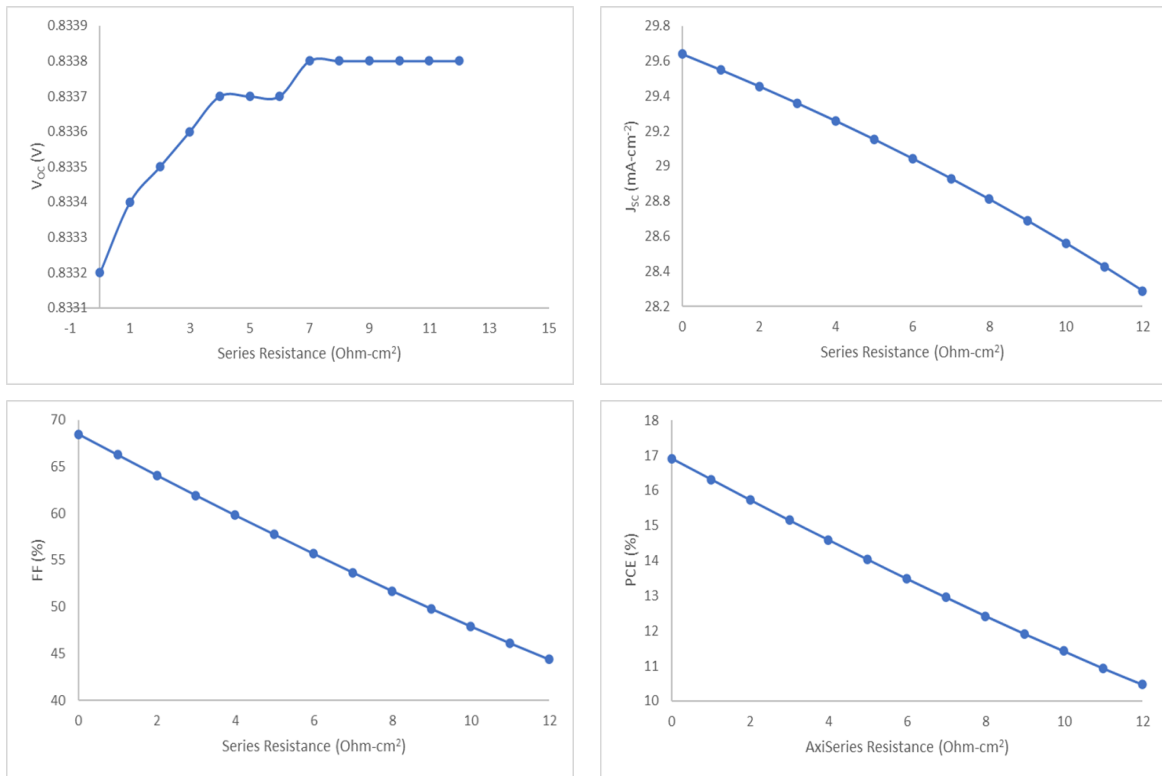


FIG. 8. Illustrates the effect of series resistance on PSC performance

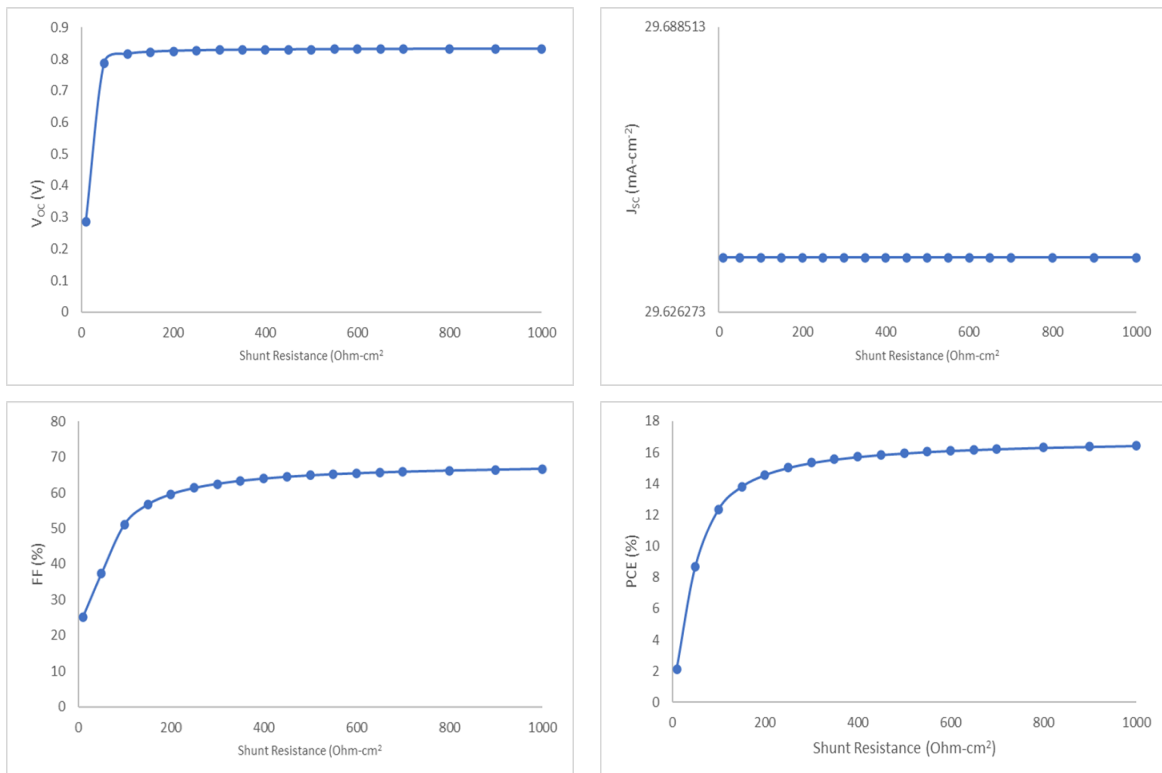


FIG. 9. Illustrates the influence of shunt resistance on PSC performance

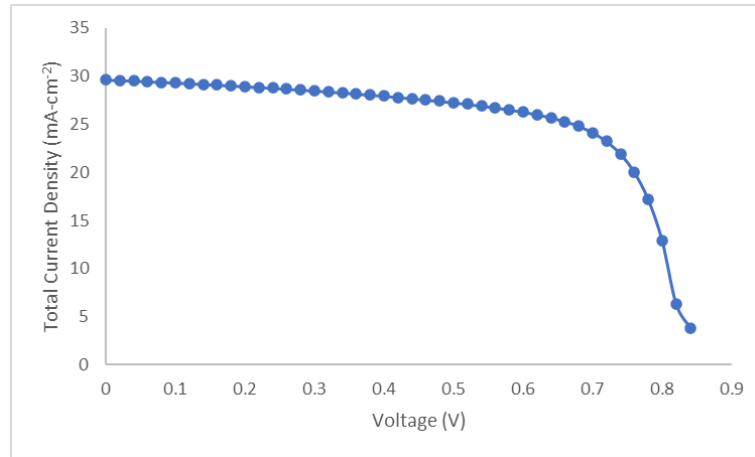


FIG. 10. Variations in short-circuit photocurrent density and open-circuit photovoltage of the investigated solar cell at $T = 300$ K

3.10. Quantum efficiency (QE)

The QE of a PSC measures the current produces when exposed to photons of specific wavelengths. Fig. 11 provides an illustration of the QE curve for a perovskite solar cell, encompassing wavelengths ranging from 300 to 900 nm. Remarkably, the QE values consistently exceed 90 % across most of this spectrum. Upon closer examination of the graph, it becomes apparent that QE increases as the wavelength extends from 300 to 390 nm. QE maintains a consistently high level exceeding 90 % up to wavelengths equal to 400 nm. However, beyond this threshold, QE gradually declines, exhibiting reduced values as the wavelength extends further to wavelengths equal to 900 nm.

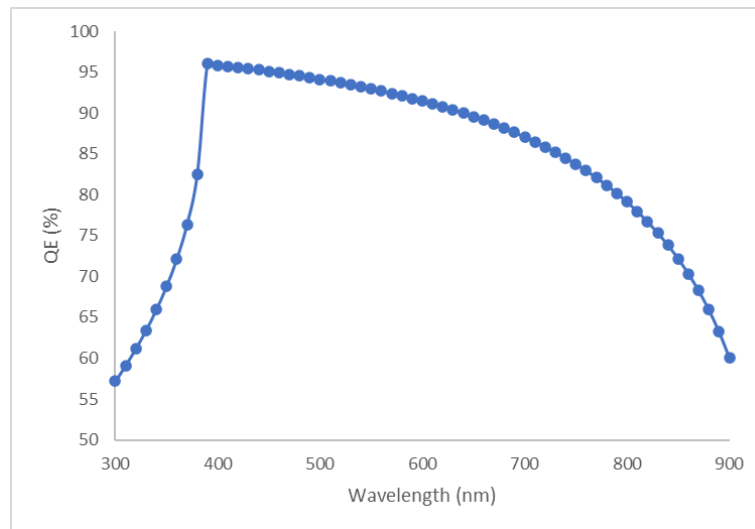


FIG. 11. Quantum efficiency curve of studied solar cell

4. Conclusion

We conducted SCAPS-1D simulations to investigate the performance of ETM in lead-free PSCs. We systematically tested various ETL materials to identify the one that offers the best solar cell performance. Subsequently, we identified the optimal ETL material. Furthermore, we independently adjusted the thickness of both the ETL and the absorber layer, along with fine-tuning the working temperature and resistances within the solar cell circuit. The outcomes of these simulations revealed significant results, showcasing the following critical performance metrics for the solar cell: V_{OC} of 0.83 V, J_{SC} of $29.63 \text{ mA}\cdot\text{cm}^{-2}$, FF of 68.48 %, and PCE of 16.91 %. Upon thorough analysis, we concluded that the most efficient configuration for the solar cell involves a ZnO (ETL) thickness of 40 nm and a $\text{CH}_3\text{NH}_3\text{SnI}_3$ (absorber layer) thickness of 500 nm. These precise dimensions resulted in the highest efficiency, offering valuable insights for optimizing future designs of lead-free perovskite solar cells.

References

- [1] Richter A., Hermle M., Glunz S.W. Reassessment of the limiting efficiency for crystalline silicon solar cells. *IEEE J. Photovolt.*, 2013, **3**, P. 1184–1191.
- [2] Sharma P., Goyal P. Evolution of PV technology from conventional to nano-materials. *Mater. Today Proc.*, 2020, **28**, P. 1593–1597.
- [3] Crabtree G.W., Lewis N.S. Physics of sustainable energy, using energy efficiently and producing it renewably. *Proceedings of the AIP Conference*, Berkeley, CA, USA, 1–2 March 2008; Melville, NY, USA, American Institute of Physics, 2008.
- [4] Goetzberger A., Hebling C., Schock H.W. Photovoltaic materials, history, status and outlook. *Mater. Sci. Eng. R. Rep.*, 2003, **40**, P. 1–46.
- [5] Nayeripour M., Mansouri M., Orooji F., Waffenschmidt E., ed. *Solar Cells*. IntechOpen Limited. London, UK, 2020, P. 1–50.
- [6] Saga T., Advances in crystalline silicon solar cell technology for industrial mass production. *NPG Asia Mater.*, 2010, **2**, P. 96–102.
- [7] Law M., Greene L.E., Johnson J.C., Saykally R., Yang P., Nanowire dye-sensitized solar cells. *Nat. Mater.*, 2005, **4**, P. 455–459.
- [8] Akihiro Kojima, Kenjiro Teshima, Yasuo Shirai, Tsutomu Miyasaka, Organometal Halide Perovskites as Visible-Light Sensitizers for Photovoltaic Cells. *J. of the American Chemical Society*, 2009, **131** (17), P. 6050–6051.
- [9] Best Research-Cell Efficiency Chart. URL: <https://www.nrel.gov/pv/cell-efficiency.html>.
- [10] Lin C. Stabilizing Organic-Inorganic Lead Halide Perovskite Solar Cells with Efficiency Beyond 20. *Front Chem.*, 2020, **8**, P. 592.
- [11] Bhaskar Parida, Arjun Singh, Abdul Kareem Kalathil Soopy, Sambasivam Sangaraju, Madhulita Sundaray, Satrujit Mishra, Shengzhong (Frank) Liu, Adel Najar. Recent Developments in Upscalable Printing Techniques for Perovskite Solar Cells. *Adv. Sci.*, 2022, **9**, 2200308.
- [12] Terry Chien-Jen Yang, Peter Fiala, Quentin Jeangros, Christophe Ballif. High-Bandgap Perovskite Materials for Multijunction Solar Cells. *Joule*, 2018, **2** (8), P. 1421–1436.
- [13] Julianna Panidi, Dimitra G. Georgiadou, Theresa Schoetz, Themis Prodromakis. Advances in Organic and Perovskite Photovoltaics Enabling a Greener Internet of Things. *Adv. Funct. Mater.*, 2022, **32**, 2200694.
- [14] Li W., Jiang Q., Yang J., Luo Y., Li X., Hou Y., Zhou S. Improvement of photovoltaic performance of perovskite solar cells with a ZnO/Zn₂SnO₄ composite compact layer. *Sol Energy Mater Sol Cells*, 2017, **159**, 143.
- [15] Ye T., Xing J., Petrovic M., Chen S., Chellappan V., Subramanian G.S., Sum T.C., Liu B., Xiong Q., Ramakrishna S. Temperature effect of the compact TiO₂ layer in planar perovskite solar cells: an interfacial electrical, optical and carrier mobility study. *Sol Energy Mater Sol Cells*, 2017, **163**, 242.
- [16] Apostolopoulou A., Sygkridou D., Rapsomanikis A., Kalarakis A.N., Stathatos E. Enhanced performance of mesostructured perovskite solar cells in ambient conditions with a composite TiO₂-In₂O₃ electron transport layer. *Sol Energy Mater Sol Cells*, 2017, **166**, 100.
- [17] Huang X., Hu Z., Xu J., Wang P., Wang L., Zhang J., Zhu Y. Low-temperature processed SnO₂ compact layer by incorporating TiO₂ layer toward efficient planar heterojunction perovskite solar cells. *Sol Energy Mater Sol Cells*, 2017, **164**, 87.
- [18] Amrit Kumar Mishra, Shukla R.K. Simulation of photovoltaic material (donor blends PTB7:PC70BM) polymer for solar cell application. *Materials Today: Proceedings*, 2021, **46** (6), P. 2288–2293.
- [19] Amrit Kumar Mishra, Shukla R.K. Effect of Humidity in the Perovskite Solar Cell. *Materials Today: Proceedings*, 2020, **29**, P. 836–838.
- [20] Amrit Kumar Mishra, Shukla R.K. Fabrication and Characterization of Perovskite (CH₃NH₃PI₃) Solar Cells. *SN Applied Sciences*, 2020, **2**, 321.
- [21] Shukla R.K., Amrit Misra. Tuning of Perovskite material for Solar Cell Application. *Int. J. of Latest Trends in Engineering and Technology*, 2019, **13** (3), P. 28–33.
- [22] Decock K., Khelifi S., Burgelman M. Modelling multivalent defects in thin film solar cells. *Thin Solid Films*, 2011, **519**, P. 7481–7484.
- [23] Burgelman M., Marlein J. Analysis of graded band gap solar cells with SCAPS. *Proceedings of the 23rd European Photovoltaic Solar Energy Conference*, 2008, Valencia, P. 2151–2155.
- [24] Verschraegen J., Burgelman M. Numerical modeling of intra-band tunneling for heterojunction solar cells in SCAPS. *Thin Solid Films*, 2007, **515**, P. 6276–6279.
- [25] Yuxiang W., Juan L., Jian X., Yangyang D., Like H., Jian N., Hongkun C., Jianjun Z. Organic-inorganic hybrid CH₃NH₃PbI₃ perovskite materials as channels in thin-film field-effect transistors. *RSC Advances*, 2016, **6**, P. 16243–16249.
- [26] Sidra Khatoun, Vishwadeep Chakraborty, Satish Kumar Yadav, Sujata Diwakar, Jyotsna Singh, Rajendra Bahadur Singh. Simulation study of CsPbI₃Br_{1-x} and MAPbI₃ heterojunction solar cell using SCAPS-1D. *Solar Energy*, 2023, **254**, P. 137–157.
- [27] Rai N., Rai S., Singh P.K., et al. Analysis of various ETL materials for an efficient perovskite solar cell by numerical simulation. *J. Mater. Sci.: Mater. Electron*, 2020, **31**, P. 16269–16280.
- [28] Patel P.K. Device simulation of highly efficient eco-friendly CH₃NH₃SnI₃ perovskite solar cell. *Sci. Rep.*, 2021, **11**, 3082.
- [29] Tiwari P., Alotaibi M.F., Al-Hadeethi Y., Srivastava V., Arkook B., Sadanand, Lohia P., Dwivedi D.K., Umar A., Algadi H., et al. Design and Simulation of Efficient SnS-Based Solar Cell Using Spiro-OMeTAD as Hole Transport Layer. *Nanomaterials*, 2022, **12**, 2506.
- [30] Parvesh K. Deendyala, Shweta Dhakla, Harpreet, Sarvesh Kumar, Manish K. Kashyap. Suitability of LBSO/CuI as an Effective ETL/HTL for Perovskite Solar Cells: A Dry Lab Approach. *Indian J. of Pure & Applied Physics*, 2023, **61**, P. 931–933.
- [31] Faiza Azri, Afak Meftah, Nouredine Sengouga, Amjad Meftah. Electron and hole transport layers optimization by numerical simulation of a perovskite solar cell. *Solar Energy*, 2019, **181**, P. 372–378.
- [32] Medina J.C.Z., Andrés E.R., Ruíz C.M., Espinosa E.C., Yarce L.T., Galeazzi Isasmendi R., Trujillo R.R., Salgado G.G., Solis A.C., Caballero F.G.N. Numerical Simulation and Performance Optimization of a Solar Cell Based on WO₃/CdTe Heterostructure Using NiO as HTL Layer by SCAPS 1D. *Coatings*, 2023, **13**, 1436.
- [33] Raoui Y., Ez-Zahraouy H., Tahiri N., El Bounagui O., Ahmad S., Kazim S. Performance analysis of MAPbI₃ based perovskite solar cells employing diverse charge selective contacts: Simulation study. *Sol. Energy*, 2019, **193**, P. 948–955.
- [34] Zapukhlyak Z.R., Nykyryu L.I., Rubish V.M., Wisz G., Prokopiv V.V., Galushchak M.O., Lishchynskyy I.M., Katanova L.O., Yavorskyi R.S. SCAPS Simulation of ZnO/CdS/CdTe/CuO Heterostructure for Photovoltaic Application. *Physics and Chemistry of Solid-State*, 2020, **21** (4), P. 660–668.
- [35] Singh A.K., et al. Performance optimization of lead free-MASnI₃ based solar cell with 27 % efficiency by numerical simulation. *Opt. Mater.*, 2021, **117**, 11193.
- [36] Hossain M.K., Rubel M.H.K., Toki G.F.I., Alam I., Rahman M.F., Bencherif H. Deep Insights into the Coupled Optoelectronic and Photovoltaic Analysis of Lead-Free CsSnI₃ Perovskite-Based Solar Cell Using DFT Calculations and SCAPS-1D Simulations. *ACS Omega*, 2022, **7** (47), P. 43210–43230.

Information about the authors:

R. K. Shukla – Physics Department, Lucknow University, Lucknow-226007, India; ORCID 0000-0001-8505-963; rajeshkumarshukla00@gmail.com

Anchal Srivastava – Physics Department, Lucknow University, Lucknow-226007, India; ORCID 0000-0002-2588-5541; asrivastava.lu@gmail.com

Shikha Rani – Physics Department, Lucknow University, Lucknow-226007, India; ORCID 0009-0003-3326-0706; shikharani0395@gmail.com

Nidhi Singh – Physics Department, Lucknow University, Lucknow-226007, India; ORCID 0009-0004-6393-2056; nidhisingh1396@gmail.com

Vishnu Kumar Dwivedi – Physics Department, Lucknow University, Lucknow-226007, India; ORCID 0000-0001-6698-7598; vishnudmts@gmail.com

Sharda Pandey – Physics Department, Lucknow University, Lucknow-226007, India; ORCID 0000-0001-9950-1195; sharda2012536@gmail.com

Navina Wadhvani – Physics Department, Lucknow University, Lucknow-226007, India; ORCID 0009-0005-0465-0486; navinawadhvani@gmail.com

Declaration of Competing Interest: The authors declare that they have no known competing financial interests or personal relationships that could have appeared to influence the work reported in this paper.

Conflict of interest: The authors declare no conflict of interest.